KfK 4220
Mai 1987

A Measurement of the Density and Compressibility of (U, Pu)-mixed Oxide at 3432 kJ/kg (7356 K)

W. Breitung, K. O. Reil
Institut für Neutronenphysik und Reaktortechnik
Projekt Schneller Brüter

Kernforschungszentrum Karlsruhe

KERNFORSCHUNGSZENTRUM KARLSRUHE
Institut für Neutronenphysik und Reaktortechnik
Projekt Schneller Brüter

KfK 4220

A measurement of the density and compressibility of (U,Pu)-mixed oxide at 3432 kJ/kg (7356 K)

W. Breitung
K.O. Reil*

*Sandia Nat. Laboratories, Org. 6423, P.O. Box 5800, Albuquerque, NM, 87185, USA

Kernforschungszentrum Karlsruhe GmbH, Karlsruhe

Kernforschungszentrum Karlsruhe GmbH
Postfach 3640, 7500 Karlsruhe 1

ISSN 0303-4003

A measurement of the density and compressibility of (U,Pu)-mixed oxide at 3432 kJ/kg (7356 K)

Abstract

In a transient in-pile heating test the density of liquid (U,Pu)-mixed oxide at 3432 $\pm$ 103 kJ/kg was measured to be 5027 $\pm$ 132 kg/m^3. The corresponding temperature is estimated to 7356 $\pm$ 212 K. The isothermal compressibility of the mixed oxide was evaluated to 2.85($\pm$ 1.65)·10^{-4}/MPa at the same temperature.

Based on these new data and previously existing measurements, new relations are proposed for the following properties of liquid UO_2 and $(U,Pu)O_2$, as well: density - enthalpy, density - temperature, thermal expansion - temperature, and isothermal compressibility - temperature.

Messung der Dichte und Kompressibilität von (U,Pu)-Mischoxid bei 3432 kJ/kg (7356 K)

Zusammenfassung

In einem transienten in-pile Test, wurde die Dichte von flüssigem (U,Pu)-Mischoxid bei 3432 $\pm$ 103 kJ/kg zu 5027 $\pm$ 132 kg/m^3 gemessen. Die entsprechende Temperatur wurde auf 7356 $\pm$ 212 K abgeschätzt. Die isotherme Kompressibilität von Mischoxid wurde zu 2.85($\pm$ 1.65)·10^{-4}/MPa bei derselben Temperatur gemessen.

Basierend auf diesen neuen Daten und bisher bestehenden Messungen, wurden neue Relationen für die folgenden Eigenschaften von flüssigem UO_2 als auch $(U,Pu)O_2$ vorgeschlagen: Dichte - Enthalpie, Dichte - Temperatur, thermische Ausdehnung - Temperatur, und isotherme Kompressibilität - Temperatur.

Contents

1. INTRODUCTION

Thermophysical properties of liquid (U,Pu)-mixed oxides are of interest for LMFBR accident analysis and for reactor safety related experiments which explore liquid fuel behaviour. This paper presents the first experimental results for the density and compressibility of liquid uranium-plutonium mixed oxide.

2. MEASUREMENT PRINCIPLE

The in-pile test described here belonged to the Effective-Equation-of-State (EEOS) series which was performed in the Annular Core Research Reactor (ACRR) at Sandia Nat. Laboratories /1/. The experiment was primarily designed to measure the saturation vapor pressure of (U,Pu)-mixed oxide.

The powdered test fuel was enclosed in a constant test volume one side of which was coupled to a pressure transducer (Fig. 1). The test fuel was then fission heated during an ACRR power excursion (7 ms FWHM) from 290 K to around 8000 K. During this temperature excursion the pressure transducer continuously monitored the increasing saturation vapor pressure in the test volume. Fig. 2 shows the measured pressure signal for experiment EEOS-09.

Around .311 seconds a very rapid pressure excursion occurred. It is believed that at this moment the expanding liquid fuel had completely filled the free space in the test volume. The still on-going heating of the liquid fuel then generated a large liquid phase pressure with a very fast rise time.

At the onset of this pressure excursion the liquid fuel density was equal to the liquid fuel mass divided by the test volume. The corresponding fuel enthalpy was evaluated as described in Section 3.3.

The rise rate of the single phase pressure contains information about the fuel compressibility.

3. DATA BASIS

3.1 Test Fuel

The detailed composition of the (U,Pu)-mixed oxide sample is given in Table I.

Table I: Specifications of uranium-plutonium mixed oxide test fuel

Metal Isotope/(U + Pu):			Impurity contents:		
U-235	.15	atom %	Mg	< 3	ppm
U-238	76.83	atom %	Si	25	ppm
Pu-239	20.01	atom %	V	< 5	ppm
Pu-240	2.66	atom %	Fe	95	ppm
Pu-241	.27	atom %	Cu	25	ppm
Pu-242	.08	atom %	Zn	<10	ppm
			Sr	< 5	ppm
			Mo	<10	ppm
O/(U + Pu)	2.09		Bi	< 1	ppm
Pu/(U + Pu)	23.02	atom %	H_2O	370	ppm
			C	170	ppm
			Cl	5	ppm
			F	< 5	ppm
			P	6	ppm
			S	770	ppm
			N	5	ppm

3.2 Pressure Signal

Fig. 2 depicts the pressure signal measured in test EEOS-09. The initially falling pressure is due to a radiation noise contribution. This noise signal was measured in a separate test without fuel and then substracted out of the data shown in Fig. 2.

Between about .3080 and .3103 seconds the pressure rose in the exponential manner typical for saturation vapor pressures. However, at the 20 and 25 MPa level two events caused negative deviations from the expected pressure signal. These events were probably extrusion of liquid fuel into the gap between crucible and piston (at 20 MPa) and a temporary freezing and binding of these parts (at 25 MPa). There is no direct proof for this hypothesis but similar pressure signals could be observed and correlated with fuel loss in earlier tests.

At .3112 seconds a very rapid pressure excursion freed the partially bounded transducer and drove it into saturation. This event is interpreted in the following discussion as a single phase liquid pressure excursion. It was caused by complete filling of the available void space with liquid fuel and further heating of this "hard" system. Failure of the transducer membrane did not occur because the signal recovered at later times from the saturation and returned close to zero. Also the post-test examination showed no sign of rupture or mechanical deformation. For these reasons there is no other mechanism than single phase liquid pressures visible which could generate such rapid and large pressure signals.

The measured time-pressure data points of this single phase pressure excursion are listed in columns 1 and 2 of Table II.

Table II: Data for single phase liquid pressure excursion in experiment EEOS-09

time (s)	pressure (MPa)	fuel enthalphy (kJ/kg)	fuel temperature (K)	fuel density (kg/m3)
.31105	29.53	3353.6	7194	5177
.31110	29.85	3379.6	7248	5127
.31115	30.20	3405.6	7302	5077
.31120	30.55	3431.6	7356	5027
.31125	44.70	3457.6	7409	4978
.31130	58.99	3483.0	7462	4929
.31135	58.99	3508.0	7514	4881
.31140	58.99	3532.9	7565	4834

3.3 Fuel Enthalpy

The time and space dependent fuel enthalpy was evaluated from the following one-dimensional model for the fission energy deposition process.

The accumulated fuel enthalpy at time t in a fuel volume element of thickness dx at location x is:

$$h(x,t) = h^{cal} \cdot \frac{I^{09}}{I^{cal}} \cdot \frac{c(x)dx}{\int_0^d c(x)dx} \cdot \frac{\int_0^t i(t)dt}{\int_0^\infty i(t)dt} \qquad (1)$$

The four terms in Eq. 1 have the following significance:

1. The first term h^{cal} is the total fuel enthalpy which was measured in a separate calibration test. In this experiment the Zircalloy crucible in the pressure cell (Fig. 1) was replaced with a thermally isolated aluminum calorimeter. This calorimeter contained the same mass of test fuel in the same geometric arrangement as the actual experiment EEOS-09. The calorimeter assembly was irradiated with an ACRR pulse of known size. From the measured temperature increase of the calorimeter the deposited total enthalpy h^{cal} (kJ/kg) was deduced.

2. The ratio I^{09}/I^{cal} scales the size of the ACRR pulse used in the calibration experiment to that of the actual test EEOS-09. The ACRR pulse size is evaluated by integrating the current of a given fission chamber, e.g.:

$$I^{09} = \int_0^\infty i^{09}(t)\,dt \qquad (2)$$

where $i^{09}(t)$ = fission chamber current measured in experiment EEOS-09.

3. The third term in Eq. (1) describes the energy deposition gradient within the fuel sample which is due to the neutron flux depression. Values for c(x) were extracted from two dimensional (r-z) neutron transport calculations using the

Los Alamos code TWODANT, installed at Sandia Nat. Laboratories. The relative quantity c(x) describes the deviation of the fuel enthalpy at location x from the average enthalpy of the whole fuel sample. The upper integration limit d represents the fuel thickness in the one dimensional model.

4. The product of the first two terms gives the average energy deposition into the EEOS-09 test fuel (kJ/kg). The third term describes the distribution of this energy in space and the fourth term in Eq. (1) the distribution in time.

Eq. (1) was used to evaluate the fuel enthalpy as function of time t and location x. Fig. 3 shows the results up to .3112 seconds. The fuel center line is located at x = 0, the fuel/crucible interface at x = d = .79 mm. Fuel melting began at .3073 seconds. The top line in Fig. (3) shows the calculated fuel enthalpy distribution at the onset of the liquid phase pressure excursion. There is a .028 mm thick crust of frozen fuel between the liquid fuel core and the Zircalloy crucible at this time. The calculated enthalpy in the liquid fuel varied between 3326 and 3619 kJ/kg. The volumetric average of 3432 kJ/kg was used for the density evaluation at .3112 seconds. Table II shows in column 3 the average liquid fuel enthalpy at times shortly before and after the onset of the pressure excursion.

The pressure-enthalpy correlation resulting from the measured pressure signal p(t) and the evaluated enthalpy h(t) is plotted in Fig. 4.

3.4 Post-Test Examination

The EEOS-09 pressure cell (Fig. 1) was disassembled after the ACRR irradiation to investigate the fuel distribution in the free volume inside the cell.

It was found that liquid fuel had extruded downwards into the slightly conical gap between piston and crucible, then radially outwards between the crucible and the Al shim, and also to some extent into the gap between crucible and outer pressure vessel.

It is not possible to specify the time of fuel extrusion, but the volume which was available for the thermal fuel expansion can be bounded by the following two cases:

A. All fuel found outside the crucible was lost in the two events (at 20 and 25 MPa) before the liquid pressure excursion occurred.

B. All fuel was lost from the crucible after the onset of liquid phase pressures, driven by the liquid pressurization.

In case A the fuel expansion volume included the volume of the external gaps outside the test volume in which fuel was found. In case B the fuel could only expand into the free space inside the crucible.

The total volume of all external fuel filled gaps could be calculated quite precisely because of two reasons. Firstly, the free volume outside the crucible was specifically designed to be as small as possible by using very tight tolerances on all internal parts of the pressure cell. Secondly, in a Quality Assurance program the actual dimensions of all fabricated parts were measured to within $\pm$ .005 mm ($\pm$.2 mil). The total gap volume outside the crucible filled with fuel was found to be only 5.2% of the test volume inside the crucible. Therefore, the above two limiting cases A and B allow a reasonably precise evaluation of the liquid fuel density.

4. DATA EVALUATION

4.1 Fuel density

4.1.1 The ρ-h data

The liquid fuel density at the onset of the liquid phase pressure (.31120 seconds) was calculated from

$$\rho_l = m_l/V_l \quad (3)$$

$$V_l = V_{tot} - V_s \quad (4)$$

$$m_l = m_{tot} - m_s \quad (5)$$

with

ρ_l = liquid fuel density (kg/m^3)

V_l = volume filled with liquid fuel (m^3)

V_{tot} = total volume
= $.19989 \cdot 10^{-6}$ m³ in case A (test volume + gaps)
= $.19000 \cdot 10^{-6}$ m³ in case B (test volume only)
V_s = volume of solid crust = $.6651 \cdot 10^{-8}$ m³ on crucible walls (Fig. 3)
m_l = mass of liquid fuel
m_{tot} = total fuel mass = $1.0128 \cdot 10^{-3}$ kg
m_s = mass of solid crust = $.668 \cdot 10^{-4}$ kg

The resulting density is ρ = 4895 kg/m³ for case A, and 5159 kg/m³ for case B. These two values correspond to 5027 $\pm$ 132 kg/m³.

The average enthalpy ($h-h_{298}$) in the liquid fuel zone at .3112 s was evaluated to 3432 $\pm$ 103 kJ/kg. The resulting ρ-h data field is shown in Fig. 5 together with the only two other density measurements on liquid oxide fuels /7,8/.

4.1.2 Recommended ρ-h function

The ρ-T measurements of Christensen /7/ and Drotning /8/ were convertered from the temperature to enthalpy format using the ANL h-T relation for liquid UO_2:

$$h-h_{298} = 1398.6 + .48495\,(T-3120) \text{ kJ/kg} \qquad (6)$$

The recommended $\rho(h)$ function shown in Fig. 5 is a straight line between Drotnings density of 8860 kg/m³ at 3120 K and the average value from this work of 5027 kg/m³ at 3432 kJ/kg. The upper and lower limit of the shaded estimated uncertainty band cover the two data fields around 1400 and 3400 kJ/kg. The recommended $\rho(h)$ function including the uncertainty band is:

$$\rho(h-h_{298}) = 8860.\,(\pm 120) - 1.885\,(\pm .106) \cdot \left\{(h-h_{298}) - 1398.6\right\} \qquad (7)$$

for $(h-h_{298})$ = 1400...3700 kJ/kg

The upper density limit is described by the + signs, and the lower limit by the - signs in Eq. (7).

The recommended ρ(h) function of Eq. (7) is compared in Fig. 6 to earlier evaluations of the density of liquid UO_2 /9,3/. The temperature values given in /9/ were transformed to enthalpies using Eq. (6). The agreement between the three evaluations is quite good.

4.1.3 Recommended ρ-T function

Figure 7 compares the density measurements for liquid oxide fuels as function of temperature. In order to compare the ρ-T data of Christensen /7/ and Drotning /8/ to the present ρ-h measurement, the enthalpy of the $(U_{.77}Pu_{.23})O_{2.09}$ test fuel was converted to temperatures using:

$$T(h\text{-}h_{298}) = \left\{(h\text{-}h_{298}) - 1345\ kJ/kg\right\} / .48495\ kJ/kgK + 3053\ K \qquad (8)$$

This relation was derived for $(U_{.77}Pu_{.23})O_{2.09}$ using data recommended in the ANL property compilation (6). According to Eq. (8) the liquid fuel enthalpy of 3432 ± 103 kJ7Kg corresponds to 7356 ± 212 K. The resulting ρ-T field is shown in Fig. 7.

The recommended ρ-T fit function is again a linear connection between the Drotning value at 3120 K and the data point at 5027 kg/m^3 - 7356 K. The dotted uncertainty band in Fig. 7 covers most of the existing data. The recommended ρ-T fit function is

$$\rho(T) = 8860\ (\pm 120) - .90486\ (\pm .0504) \cdot (T\text{-}3120)\ kg/m^3 \qquad (9)$$
$$\text{for } T = 3120...8000\ K$$

The + signs in Eq. (9) give the upper limit of the shaded uncertainty band, and the - signs the respective lower limit.

The density from Eq. (9) is compared to other ρ-T evaluations in Fig. 8. The agreement is again quite good. All evaluations fall within the rather narrow uncertainty band of Eq. (9).

4.2 Thermal expansion

In a single phase region the thermal expansion coefficient

$$\alpha = \frac{1}{V} \cdot \left(\frac{\partial V}{\partial T}\right)_p \tag{10}$$

is connected to the density by the differential Equation of State

$$-\frac{d\rho}{\rho} = \alpha\, dT - \beta\, dp \tag{11}$$

where β is the isothermal compressibility of the substance. Along the saturation line dT and dp are interrelated by the Clausius– C lapeyron equation:

$$\left(\frac{dp}{dT}\right)_{sat} = \frac{\Delta h_{vap}}{T\, \Delta v_{vap}} \approx \frac{\Delta h_{vap}}{RT^2} \cdot p_{sat} \tag{12}$$

For state changes along the saturation line, the density change is

$$\frac{d\rho}{\rho} = -\left(\alpha - \frac{\beta\, \Delta h_{vap} \cdot p_{sat}}{RT^2}\right) dT \tag{13}$$

For liquid UO_2 and $(U,Pu)O_2$ the second term in the backet is much smaller than α, reaching at most a few percent of α at 8000 K. This means that along the saturation line, the volume change due to the pressure change is much smaller than the corresponding volume change due to the thermal expansion. The thermal expansion coefficient may therefore be evaluated from $\rho(T)$, which was measured under saturation conditions, according to:

$$\alpha = -\frac{1}{\rho} \cdot \frac{d\rho}{dT} \tag{14}$$

Eq. (14) is the incompressible substance approximation of Eq. (11). It is correct for liquid UO_2 and $(U,Pu)O_2$ up to around 8000 K within a few percent. Eq. (9) was used for the evaluation of the thermal expansion coefficient α of liquid $(U,Pu)O_2$.

Fig. 9 summarizes the data for the thermal expansion coefficient of liquid oxide fuels.

4.3 Isothermal compressibility

In the single phase region of a substance the differential Equation-of-State may be written as

$$\frac{dv}{v} = \alpha \; dT - \beta \; dp \qquad (15)$$

where

dv/v = relative change in molar volume v in going from state 1 to state 2,
α = $1/v\,(\delta v/\delta T)_p$ = thermal expansion coefficient,
dT = temperature change between states 1 and 2,
β = $-1/v\,(\delta v/\delta p)_T$ = isothermal compressibility,
dp = pressure change between states 1 and 2.

Eq. (7) simply states that the net volume change due to a change of state by dT and dp is equal to the volume increase from thermal expansion minus the volume decrease due to the materials compression.

If one interprets the fast pressure rise in EEOS-09 as a single phase liquid pressure, the fuel compressibility may be deduced from

$$\beta = \alpha \cdot \frac{T_2 - T_1}{p_2 - p_1} - \frac{\Delta v / v}{p_2 - p_1} \qquad (16)$$

The index 1 refers to the onset of the liquid phase pressure and the index 2 refers to the next data point on the pressure ramp (fourth and fifth point in Table II and Fig. 4).

According to Eq. (14), the thermal expansion α at state 1 (and 2) can be evaluated from the measured liquid density given in Eq. (9):

$$\alpha = -\frac{1}{\rho} \cdot \left.\frac{d\rho}{dT}\right|_{T=7356K} = 1.80 \cdot 10^{-4} \; \frac{1}{K} \qquad (17)$$

The fuel temperature increase T_2-T_1 was 53 K, and the measured pressure increase p_2-p_1 was 14.15 MPa (Table II). The fuel volume v increased in going from state 1 to state 2 because the transducer membrane yielded slightly under the increased pressure.

In a separate out-of-pile loading test the volume change per unit pressure increase was measured by applying a known force to the transducer membrane and measuring its deflection. It was found that the test volume increase caused by the transducer travel is:

$$\Delta v/v = 2.2 \cdot 10^{-4}\ 1/\mathrm{MPa} \cdot (p_2 - p_1) \qquad (18)$$

With the above values the fuel compressibility at 7356 K becomes $\beta = 4.5 \cdot 10^{-4}$/MPa.

This value for β was derived from the slope of the liquid phase pressure excursion (Fig. 4). The time between successive data points in Fig. 4 is $5 \cdot 10^{-5}$ seconds. Due to this finite time step in the measurement one can in principle envision pressure excursions with a rise time faster than $10 \cdot 10^{-5}$ s which would result in the same data points as shown in Fig. 4. However, if the true rise time should have been shorter than the sampling intervall of $5 \cdot 10^{-5}$ s, it would have been quite unlikely to measure a data point midway along the ramp. More likely there would have been no or only one point close to the initial or final pressure level.

To cover this uncertainty from the finite sampling time of the data aquisition system, Eq. (16) was also evaluated with a pressure rise rate twice as high as depicted in Fig. 4. The resulting compressibility at 7356 K is $\beta = 1.2 \cdot 10^{-4}$/MPa. This can be considered a lower bound for the fuel compressibility. The value of $4.5 \cdot 10^{-4}$/MPa represents an upper bound for β.

The upper and lower compressibility bound is compared in Fig. 10 to two theoretical evaluations. The first one is the theoretical estimate given by Fink et al /9/. The second one is a combination of the density $\rho(T)$ recommended in Eq. (9) and the $(\delta p/\delta T)_v$-values calculated by E.A. Fischer /3/:

$$\beta = \frac{(\partial v/\partial T)_p / v}{(\partial p/\partial T)_T} = \frac{-\frac{1}{\rho} \cdot \left(\frac{\partial \rho}{\partial T}\right)_{sat}}{(\partial p/\partial T)_v} \qquad (19)$$

where from Reference /3/:

$$(\delta p/\delta T)_v = .2538 + .16391\,(\rho - 3.475) + .026561\,(\rho - 3.475)^3\ \mathrm{MPa/K} \qquad (20)$$
$$\rho = 3.475 \ldots 8.860\ \mathrm{g/cm^3}$$

The compressibility from Eqs. (19), (9), and (20) is in better agreement with the measured value than are the calculations of Fink et al.

4.4 Error estimates

4.4.1 Fuel density

The only quantity in Eqs. (3), (4), and (5) with a noticable error margin is the calculated crust thickness which was used to derive V_S and m_S. However, V_S and m_S tend to cancel each other in Eq. (3). A possible error of $\pm 20\%$ in the calculated crust thickness would result in only $\pm .8\%$ change in the fuel density.

Thermal expansion of the Zircalloy crucible also had a negligible effect.

The dominant uncertainty in the fuel density arises from the unknown timing of the fuel extrusion into gaps outside the test volume. This effect is bounded by the two cases A and B.

4.4.2 Fuel enthalpy

Each of the four terms in Eq. (1) contributes in principle to the total error in the fuel enthalpy evaluation.

The uncertainty in h^{cal}, which was determined in a separate calibration test, is mainly due to the uncertainty in the calorimeter heat capacity ($\pm 2\%$) and in the calorimeter temperature rise ΔT ($\pm 1\%$).

The errors in both the second and the fourth term in Eq. (1) are determined by the power-current linearity of the fission chamber. The used type of fission chamber was specified by the manufacturer to be highly linear over three orders of magnitude. Comparison of the used fission chamber with fission chambers of other sensitivities (and ranges) showed no detectable deviations from linearity /5/. The error contribution from this source was therefore considered negligible.

Because of the rather uniform enthalpy distribution in the liquid fuel (Fig. 3) the average enthalpy was correlated with the measured density. Taking the average

over the liquid fuel corresponds to integrating c(x) over x in Eq. (1). The evaluated average enthalpy is therefore independent of c(x), if the small effect of the thin solid crust is neglected. The error introduced from the third term in Eq. (1) is therefore very small.

Two additional possible error sources must be addressed, namely heat losses and systematic errors from the form of Eq. (1).

The heat loss from the test fuel was small, only a few % up to the .3120 seconds of interest here. The reasons are 1.) solid fuel powder in a vaccuum environment has a very low thermal conductivity; 2.) after fuel melting an isolating fuel crust formed on the Zr crucible, and 3.) the time from melting to the single phase pressure event was only 3.7 ms.

The heat loss models for liquid fuel conduction and convection incorporated in the enthalpy evaluation code, were benchmarked against the measured pressure decay curves of the tests EEOS-04 to -07. The good agreement between measured and calculated pressure decay signals in those tests lends some support to the heat loss models (Ref. 2, p.70). Because of the small magnitude of the heat losses and the apparently reliable modeling, the error contribution to the fuel enthalpy evaluation should be below $\pm$ 1%.

The most important presumption for the validity of Eq. (1) is that the fuel density in the test volume is constant in time and space. This assumption is based on a number of experimental and theoretical informations, which uniquely show that liquid fuel is violently agitated by the existing pressure gradients. The fuel should therefore be distributed rather homogeneously throughout the test volume during energy deposition times. The possible error from the constant-density assumption made in Eq. (1) is difficult to estimate, but for the average fuel enthalpy it should not be above $\pm$ 1 or 2%.

In summary, the total uncertainty in the average liquid fuel enthalpy from the above discussed error sources becomes $\pm$3% using the usual square root addition rule for statistically independent error sources. It should be emphasized that the average enthalpy values are purely based on measured information, they do not depend sensitively on theoretical calculations.

It should be mentioned here that the correctness of the described enthalpy evaluation procedure could be confirmed experimentally by the agreement of measured with calculated fuel melting time. Melting events were observed in test EEOS-05 (Ref. 2, Fig. VI.14) and in later experiments using an inert cover gas (EEOS-10 and 11).

4.4.3 Fuel temperature

The fuel temperature evaluation was based on Eq. (8). The dominant uncertainties in Eq. (8) is that propagated from the fuel enthalpy (+3%) and that from the heat capacity of liquid (U,Pu)-mixed oxide. The liquidus enthalpy (1345 kJ/kg) and the liquidus temperature (3053 K) are relatively well known.

The constant heat capacity value used in Eq. (8) is that recommended by Fink et al (9). It was derived from liquid UO_2 enthalpy data between 3120 and 3530 K. This is the only experimental information on c_p of liquid fuel oxides.

The most recent theoretical result is from E.A. Fischer's Significant Structures Theory (SST) model which agrees with other measured UO_2 properties like vapor pressure, thermal expansion of the liquid and isothermal compressibility (Figures 8, 9, 10). The SST result for c_p is about .473 kJ/kg K at 3120 K, .485 at 3550 K, and it reaches a flat maximum of .515 at 5400 K. c_p then falls again and reaches .485 around 7400 K. If this SST c_p instead of the ANL value is used in Eq. (8) to convert the enthalpy of 3432 kJ/kg, the temperature comes out 180 K lower (7177 K instead of 7356 K). This corresponds to an average SST c_p of .506 kJ/kg K, which is only 4.3% higher than the ANL value used in Eq. (8)..

In light of these new c_p data, which are the current best estimate, it seems not unreasonable to consider a $\pm$5% change in the heat capacity value of Eq. (8). The corresponding effect on the temperature at 7356 K would be $\pm$210 K. The width of the error band at 5000 kg/m^3 in Fig. 7 is about $\pm$350 K. The square root error addition of the c_p-effect widens the error band only by a factor 1.17. This shows that currently existing c_p uncertainties (of the order of .460 to .510 kJ/kg) do not strongly influence the estimated test fuel temperature.

4.4.4 Fuel compressibility

The rather large error margin in the derived fuel compressibility is due to the sampling time of $5 \cdot 10^{-5}$ seconds (20 kHz) used in EEOS-09. This sampling rate is adequate for the measurement of the saturation vapor pressure excursion (the primary goal of EEOS-09) but somewhat too slow for the very rapid single phase pressure ramp.

Another point that needs to be addressed is the time resolution of the pressure measuring system. The bare transducer had a cut-off frequency (-3 dB point) of about 45 kHz (Kaman Model KP-1911). In the EEOS pressure cell an additional mass of about .01 kg was coupled to the transducer membrane (mass of the Zr crucible + Al adapter, Fig. 1). It was found however in an earlier study /4/ that this should not noticeably alter the frequency response of the transducer, mainly because the forces acting on the transducer membrane are much larger than the retardation forces ($\ddot{m}x$) from the additional mass. The apparent risetime of the liquid pressure excursion in EEOS-09 (Fig. 4) corresponds to a frequency of about 10 kHz.

Therefore the mechanical response time of the pressure sensing system should have been fast enough to resolve the liquid phase pressure excursion.

The limiting factor for the compressibility evaluation was the 20 kHz sampling frequency of the data acquisition system.

4.5 Experiment EEOS-08

Experiment EEOS-08 was very similar to EEOS-09 with respect to the test fuel and experiment hardware. The main difference was that apparently no liquid fuel extruded from the crucible during the reactor pulse. No bonding of the crucible occurred and fuel vapor pressures could be measured up to 54 MPa. At this level the transducer signal became saturated and no liquid phase pressure event could be observed in EEOS-08.

From the known fuel mass, the test volume, and the fuel enthalpy at the time of transducer saturation, it was concluded that the density of liquid $(U_{.77}Pu_{.23})O_{2.09}$

at 3417 kJ/kg must be greater than 4882 kg/m^3. This confirms the density result from experiment EEOS-09.

5. Discussion

5.1 Density-enthalpy data

Fig. 5 compares this ρ-h measurement for $(U_{.77}Pu_{.23})O_{2.09}$ to the only other two density measurements on liquid oxide fuels /7,8/. The temperature values of these experiments were transformed to enthalpies using Eq. (6).

The data from these stationary measurements are limited to the first 120 kJ/kg beyond melting due to material problems. The new data point at 3432 kJ/kg extends the data basis almost 2000 kJ/kg further into the liquid regime. The fuel density at this state is only about 57% of the melt density.

The recommended ρ(h) function (Eq. 7) is a straight line between Drotnings average density at 1398.6 kJ/kg (3120 K) and the measured value at 3432 kJ/kg. Drotning's density at the UO_2 melting point 8860 kg/m^3 ($\pm$ .7%) was chosen over Christensen's value of 8740 kg/m^3 ($\pm$2%) because of the smaller error margin. Both values agree within their experimental uncertainties.

In principle the density of an oxide fuel is a function of the U isotope vector, the Pu isotope vector, the U/(U + Pu) ratio, and the O/(U + Pu) ratio. The differences between uranium and (U,Pu)-oxides are however small.

At 298 K the theoretical density of $U^{238}O_{2.00}$ and $(U^{238}{}_{.75}Pu^{239}{}_{.25})O_{2.00}$ differ only by 1%. Since also the thermal expansion of both oxides is identical within the quite small uncertainties up to the melting temperature /6/, the Pu content seems to have a negligeable effect on the density of solid oxide fuel.

The same appears to be the case in the liquid regime, if one compares the new data point from EEOS-09 with earlier density evaluations for liquid UO_2 (Fig. 6). Both evaluations for liquid UO_2 (Fink et al. 1981, and Fischer 1987) agree with the (U,Pu)-mixed oxide data point at 5027 kg/m^3 within the experimental uncertainty.

For this reason and also in view of the limited number of density data points, it appears justified to recommend the ρ(h) fit function of Eq. (7) for UO_2 and LMFBR-typical (U,Pu) mixed oxides as well. The uncertainty band given in Eq. (7), which is shown in Fig. 6 as a shaded band, should cover the relatively small effect of the Pu content on the liquid oxide density. At 1400 kJ/kg this band has a spread of $\pm$1.4% and at 3500 kJ/kg the width is $\pm$6.6%.

5.2 Density-temperature data

Fig. 7 compares the three density measurements on liquid oxide fuels in the ρ-T format. The ρ-h result from EEOS-09 was converted with Eq. (8).

The recommended ρ(T) fit function is a straight line between the EEOS-09 data point (7356 K, 5027 kg/m^3) and Drotning's average UO_2 density at the melting temperature (3120 K, 8860 kg/m^3). The shaded uncertainty band covers the EEOS-09 data field at high temperatures and the ANL recommendation for UO_2 at low temperatures. The analytical form of this band is given in Eq. (9) by the + and - sign.

Eq. (9) is compared in Fig. 8 to two earlier ρ(T) evaluations /3,9/. The very good agreement between the three evaluations is slightly influenced by the fact that both Eq. (9) and Fischer's Significant Structures Theory are anchored at Drotnings UO_2 melt density. Apart from this the three evaluations are based on independent information:

- Fink et al. used Christensens thermal expansion measurement from 3120 to 3370 K for their extrapolation,
- Fischer /3/ adjusted his Significant Structure Theory model on recent vapor pressure measurements up to 8500 K/1/, and on Drotnings liquid density value at 3120 K, and
- Eq. (9) describes the new EEOS-09 density measurement.

Fig. 8 shows that these three density evaluations are close together and well covered by the shaded uncertainty band. This band corresponds to an error margin of $\pm$8.4% at 8000 K.

It is noteworthy that the measured slope dρ/dT at the melt temperature agrees very closely with the slope of Eq. (9):

	Eq. (9)	Drotning /8/	Christensen /7/
dρ/dT (kg/m^3 / K)	.905 $\pm$ .05	.916 $\pm$ .04	.918

Within the rather narrow experimental uncertainty range, the density decrease with temperature is constant up to at least 8000 K. This indicates that the critical region, where dρ/dT approaches $-\infty$, must still be well above 8000 K. Estimates for the critical temperature T_c of UO_2 ranged in the past from 6500 to 10 000 K. It appears now that T_c values below about 9000 K could not be consistent with the new density measurement. The result of Fischer's SST calculation is T_c = 10 600 K, with ρ_c at 1560 kg/m^3.

5.3 Thermal expansion data

Fig. 9 summarizes the data for the thermal expansion coefficient of liquid oxide fuels.

Christensen /7/ measured a linear expansion coefficient in the liquid phase (3120-3370 K) of .35·10^{-4}/K which corresponds to a volumetric expansion coefficient of 1.05·10^{-4}/K.

The α values from Drotnings density relation $\rho(T) = 8860 - .916\,(T-3120)$ kg/m^3 agree very closely with Christensen's results, e.g. 1.04·10^{-4}/K at 3200 K.

Two sets of data from Fink et al. /9/ are plotted in Fig. 9. The first one is α evaluated with Eq. (14) from their recommended ρ(T) function, which is also shown in Fig. 8. The second one is α as given in their Table A1.1.10.9. These data were based on Christensen's expansion measurements between 3120 and 3370 K but their extrapolation to higher temperatures leads to increasing deviations from the other results.

The α based on the ANL density recommendation agrees within 5% with the thermal expansion coefficient from Eq. (9) and E.A. Fischer's ρ(T).

The shaded error band in Fig. 9 corresponds to the shaded band in Fig. 8, and to the + and - sign in Eq. (9). Its spread is about $\pm 6\%$ at 3120 K and $\pm 13\%$ at 8000 K. Based on the presently available experimental information it appears quite unlikely that the true expansion coefficient of UO_2 and $(U_{.75}Pu_{.25})O_2$ is outside of these error margins.

5.4 Isothermal compressibility data

Figure 10 compares the measured fuel compressibility β with two theoretical evaluations.

The prediction of Fink et al. /9/ required extrapolation of a number of thermophysical data up to 6000 K. Fink et al. estimated the possible σ-error in the result to $\pm 85\%$ at 6000 K. This uncertainty range is depicted in Fig. 10 by two arrow heads.

The results from E.A. Fischer's Significant Structures Theory approach /3/ are roughly a factor of 2 below the ANL estimate. The SST result appears to be the current best estimate for the isothermal compressibility of liquid oxide fuels for the following reasons:

1. The SST data are based on a detailed physical model, starting from basic properties of UO_2 molecules and liquid UO_2.
2. They are not in contradiction with the ANL values, and they agree with the experimental measurements.
3. The uncertainty range of the only experimental data is fairly large (1.2 to $4.5 \cdot 10^{-4}$/MPa).

6. Summary

In a transient in-pile heating test a sample of (U,Pu)-mixed oxide was heated along the saturation line. A liquid phase pressure was encountered at a fuel enthalpy of $(h-h_{298}) = 3432(\pm 103)$ kJ/kg, which corresponds to 7356 ± 212 K. From the fuel mass and known test volume a fuel density of $5027(\pm 132)$ kg/m^3 was determined. The measured rise rate of the liquid phase pressure excursion

resulted in an isothermal fuel compressibility of $2.85(\pm 1.65)\cdot 10^{-4}$/MPa at the same temperature.

Based on these new data and the stationary density measurements which exist up to 3370 K, new relations were proposed for the following properties:

1. Density-enthalpy, 1400 to 3700 kJ/kg, Eq. (7), Figures 5 and 6.
2. Density-temperature, 3120 to 8000 K, Eq. (9), Figures 7 and 8.
3. Thermal expansion-temperature, 3120-8000 K, Eq. (14) with Eq. (9), Figure 9.
4. Isothermal compressibility-temperature, 3120-8000 K, Eqs. (9), (19), (20), Figure 10.

The new density data point for liquid (U,Pu)-mixed oxide agrees very well with the extrapolation of the stationary measurements on liquid UO_2 (Fig. 8, Fink et al.). Thus the effect of the Pu content on the density of liquid oxide fuel seems to be negligeable, compared to the remaining uncertainty in the density data. It appears justified to recommend the new property relations for UO_2 and LMFBR-typical (U,Pu)-mixed oxide as well.

The new density result at 7356 K indicates that the critical temperature of liquid oxide fuel is well above 8000 K.

Acknowledgements

The authors are grateful to J. Garcia, SNL, for his help in the experiment preparation, to C.W. Tucker for assistance in the design of EEOS hardware, and to D. Pipher for the quality assurance program. The authors further acknowledge the provision of funds by the management at KfK (G. Heusener and G. Kessler) and NRC (R.W. Wright).

References:

/1/ W. Breitung and K.O. Reil, "In-pile Vapor Pressure Measurements on UO_2 and $(U,Pu)O_2$ from 4700 to 8500 K". Conf. on Science and Technology of Fast Reactor Safety, May 12-16, 1986, Guernsey, UK

/2/ W. Breitung and K.O. Reil, "In-pile Vapor Pressure Measurements on UO_2 and $(U,Pu)O_2$". Report Nucl. Research Center Karlsruhe, KfK-3939 (August 1985)

/3/ E.A. Fischer, "Evaluation of the Urania Equation of State based on recent vapor pressure measurements", Report Nucl. Research Center Karlsruhe, KfK-4084 (1987), to be published

/4/ W. Breitung, "Dynamic Response of the Pressure Transducer in EEOS Experiments", unpublished report (September 1980)

/5/ S.A. Wright, private communication (February 1987)

/6/ L. Leibowitz et al., "Properties for LMFBR Safety Analysis", Report ANL-CEN-RSD-76-1 (1976), Argonne National Laboratory, USA

/7/ J.A. Christensen, "Thermal Expansion and Change in Volume of Uranium Dioxide on Melting". J. Amer. Cer. Soc. 40 (1963) 607

/8/ W.D. Drotning, "Thermal Expansion of Molten Uranium Dioxide", Proc. 8th Symp. on Thermophysical Properties, NBS, Gaithersburg, Maryland, USA (June 15-18, 1981), CONF-810696-1

/9/ J.K. Fink, M.G. Chasanov, and L. Leibowitz, "Thermodynamic Properties of Uranium Dioxide", Report ANL-CEN-RSD-80-3 (April 1981) Argonne Nat. Laboratory, Argonne, Ill., USA

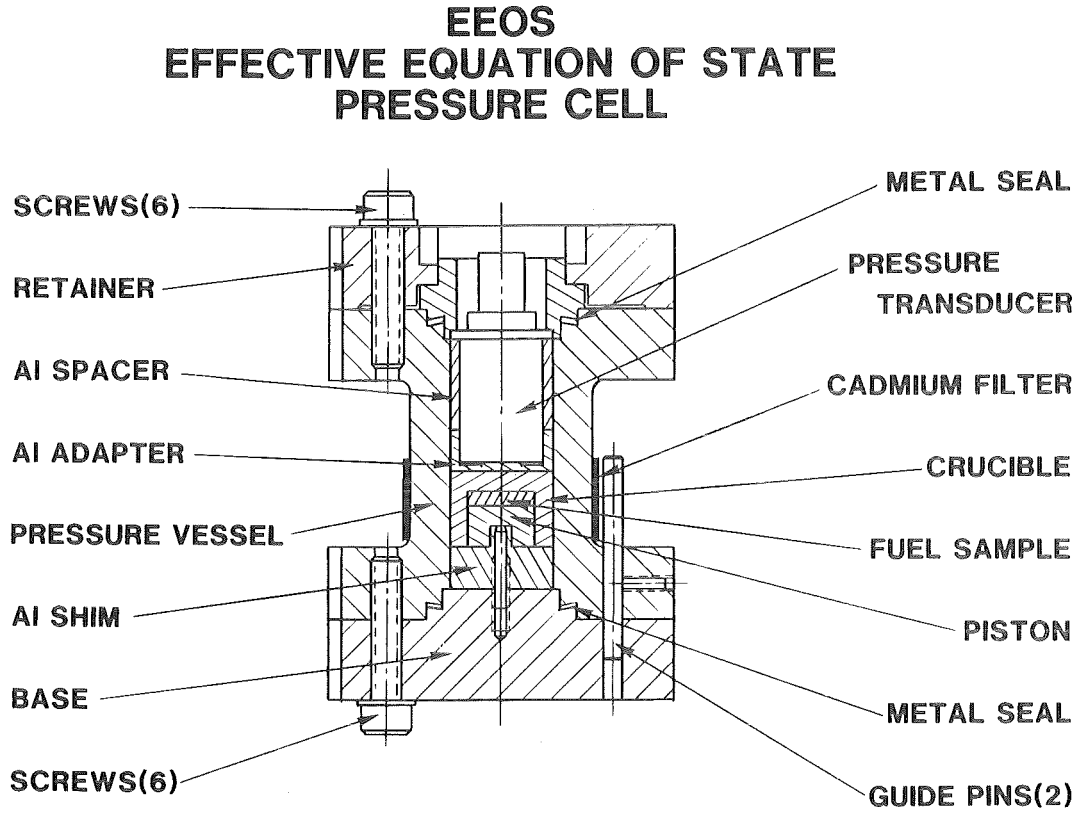

Figure 1: Design of the EEOS pressure cell. The crucible was filled with 1 g of (U,Pu)-mixed oxide powder, leaving about 52% void space in the test volume. The sample was heated from 290 K to around 8000 K in 10 milliseconds. The pressure transducer continuously monitored the pressure in the test volume.

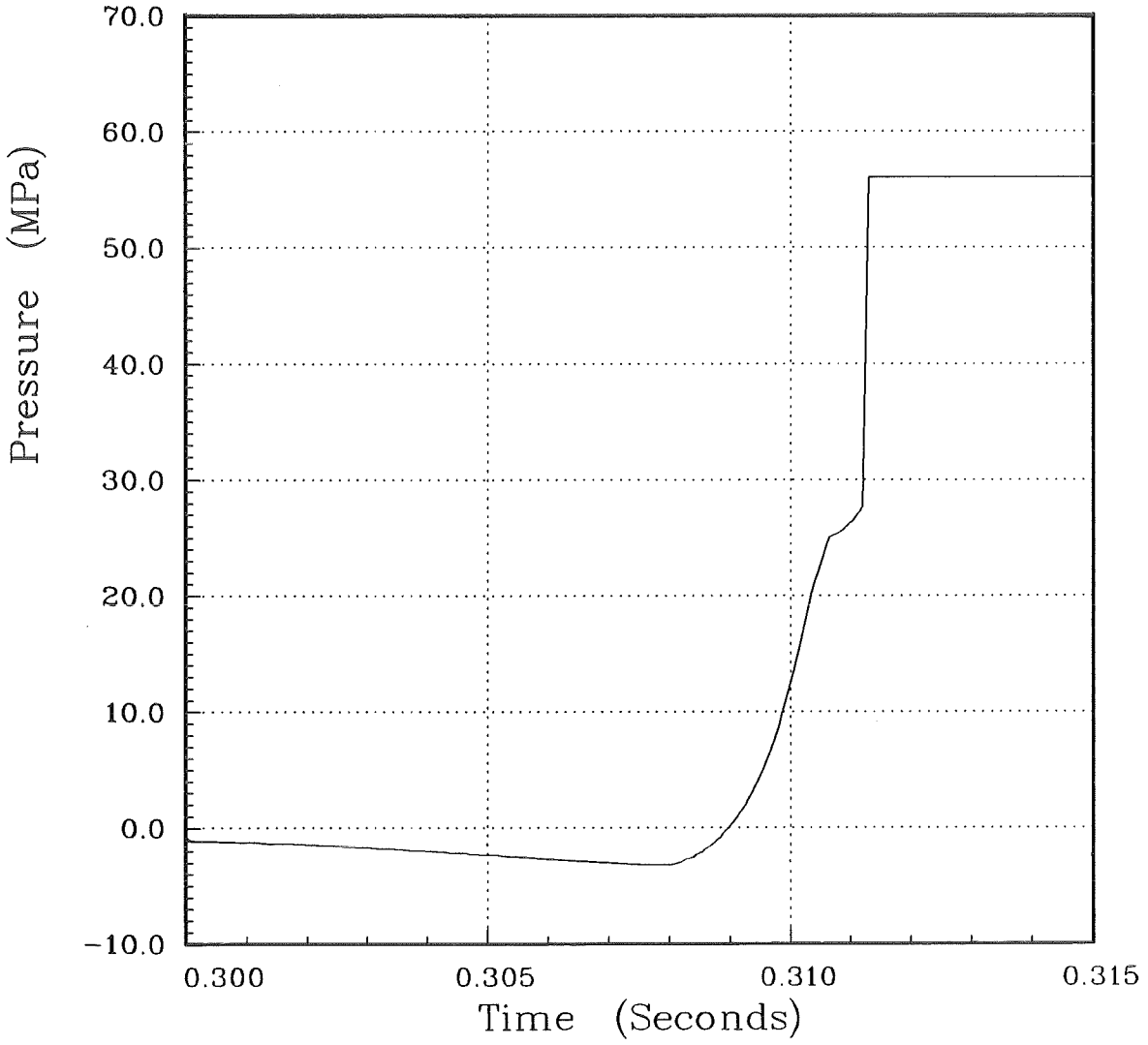

Figure 2: Pressure signal measured in test EEOS-09 (not corrected for background contribution). At .3112 seconds the fuel had more than doubled its volume due to thermal expansion, and had completely filled the test volume. Further heating of the liquid oxide generated large liquid phase pressures.

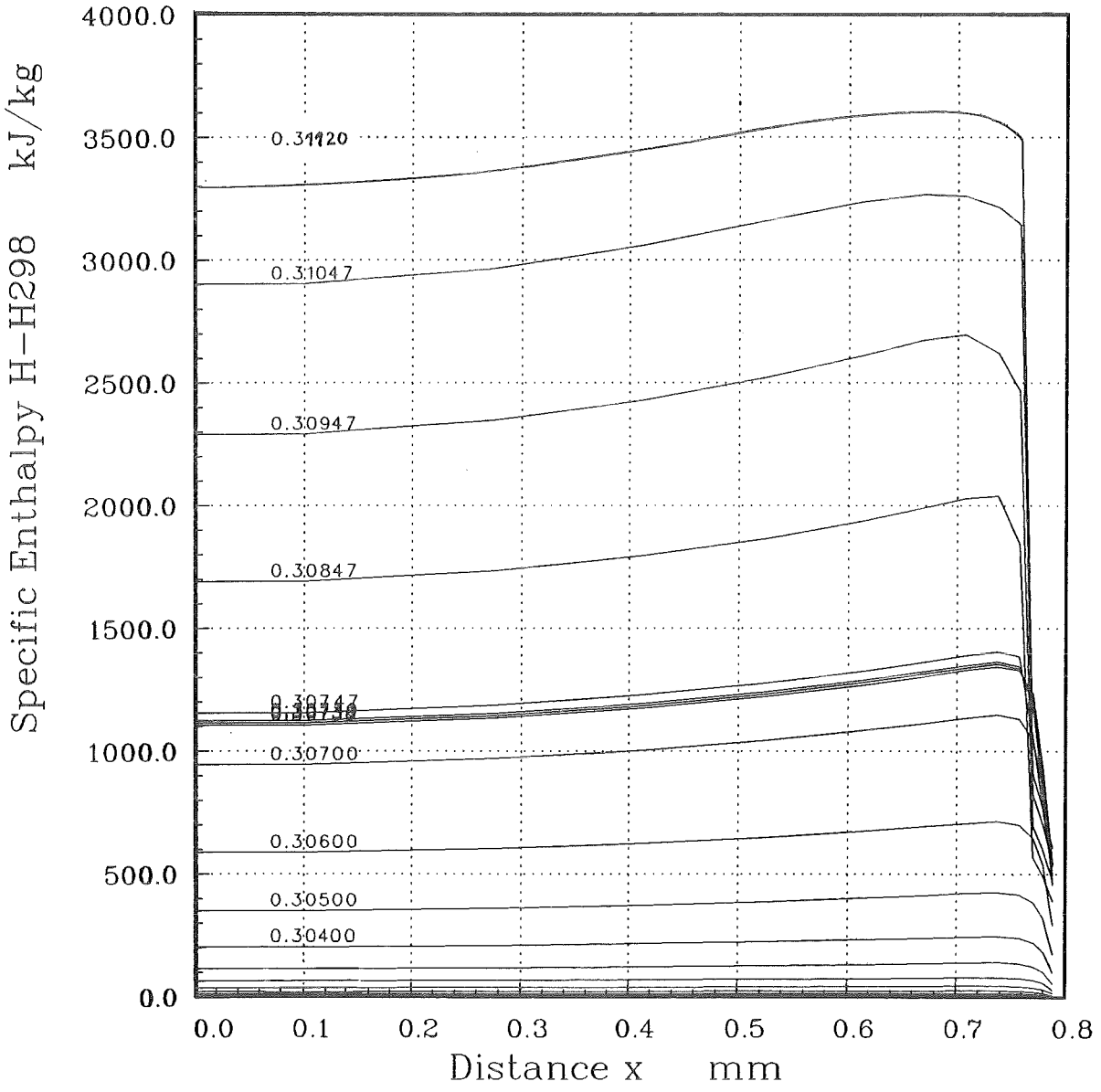

Figure 3: Results of the time and space dependent (one-dimensional) enthalpy evaluation for the (U,Pu) oxide sample up to .3112 seconds. There is a thin crust of frozen fuel between the cold crucible wall at x = .79 mm, and the liquid fuel core. The liquid fuel is heated very nearly adiabatic. The average enthalpy in the liquid was determined to 3432 $\pm$ 103 kJ/kg at .3112 seconds.

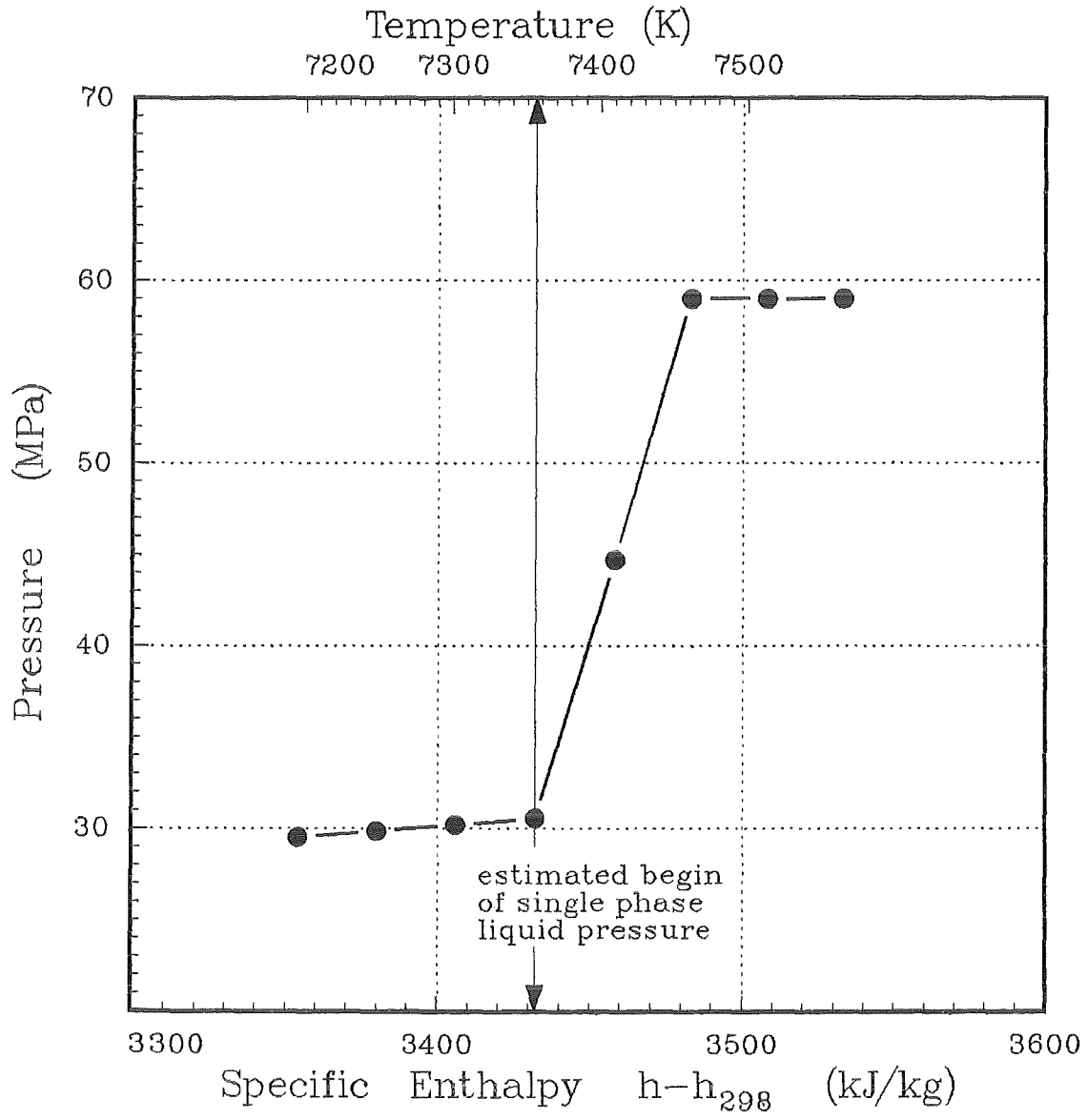

Figure 4: Pressure-enthalpy data points for the liquid phase pressure excursion which started at 3432 kJ/kg, corresponding to 7356 K. The oxide density at this point in time was 5027 ± 132 kg/m^3. The pressure transducer saturated at 59 MPa. The slope of the pressure ramp contains information about the compressibility of (U,Pu)-mixed oxide (Eq. 16).

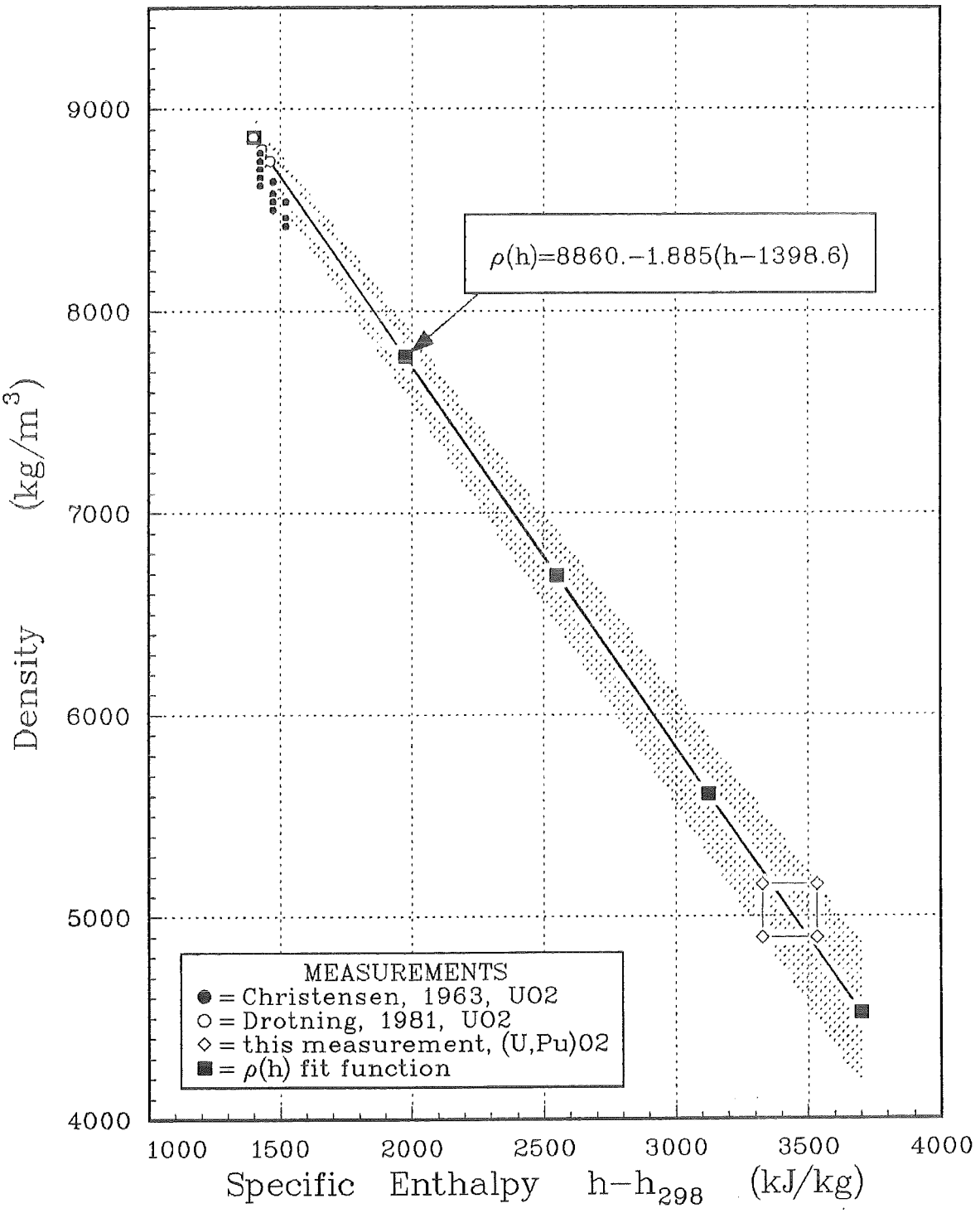

Figure 5: Comparison of new density data point at 3432 kJ/kg to the existing measurements on liquid UO_2. The new density point extends the data basis almost 2000 kJ/kg further into the liquid regime. The ρ(h) fit function is recommended for UO_2 and LMFBR typical (U,Pu)-mixed oxide as well (Eq. 7). The shaded band shows the estimated error margin of the ρ(h) fit function.

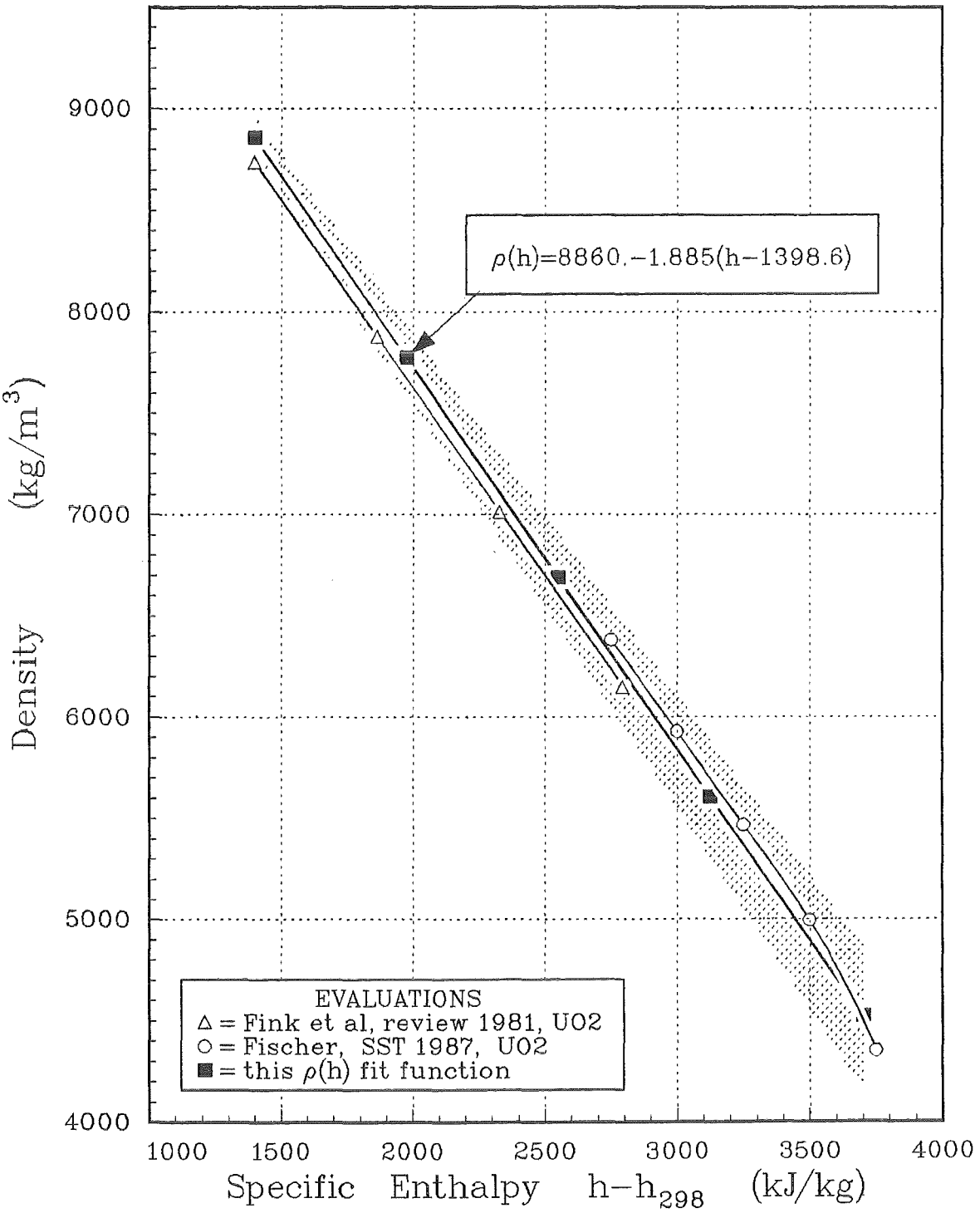

Figure 6: Comparison of the recommended ρ(h) fit function (Eq. 7) to earlier evaluations for UO_2. All relations are well covered by the estimated error band of Eq. (7). The estimated error band has a spread of $\pm$1.4% at 1400 kJ/kg and $\pm$6.6% at 3500 kJ/kg.

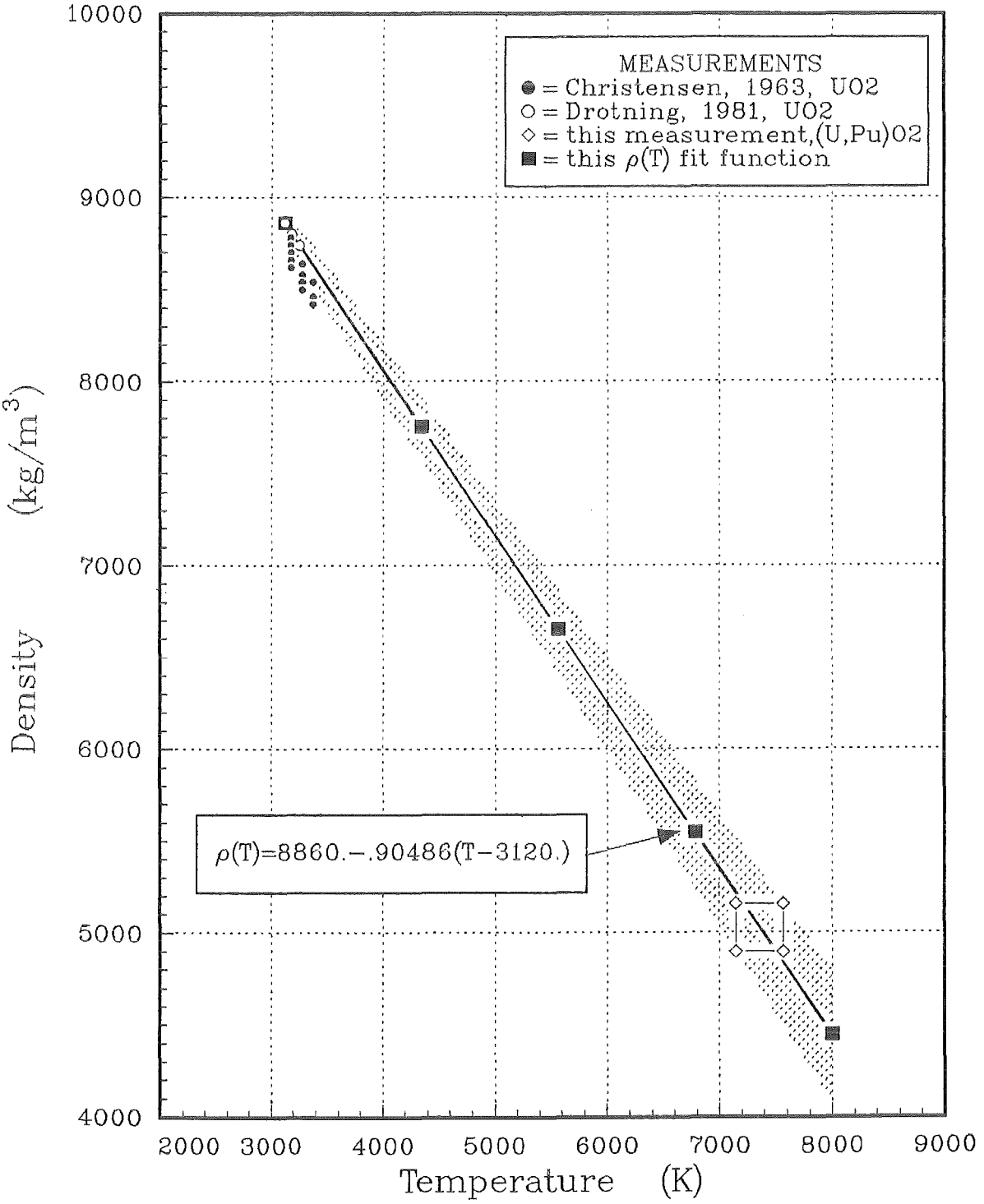

Figure 7: Comparison of the existing density measurements in the ρ-T format. The recommended ρ(T) fit function and the estimated error band is given by Eq. (9).

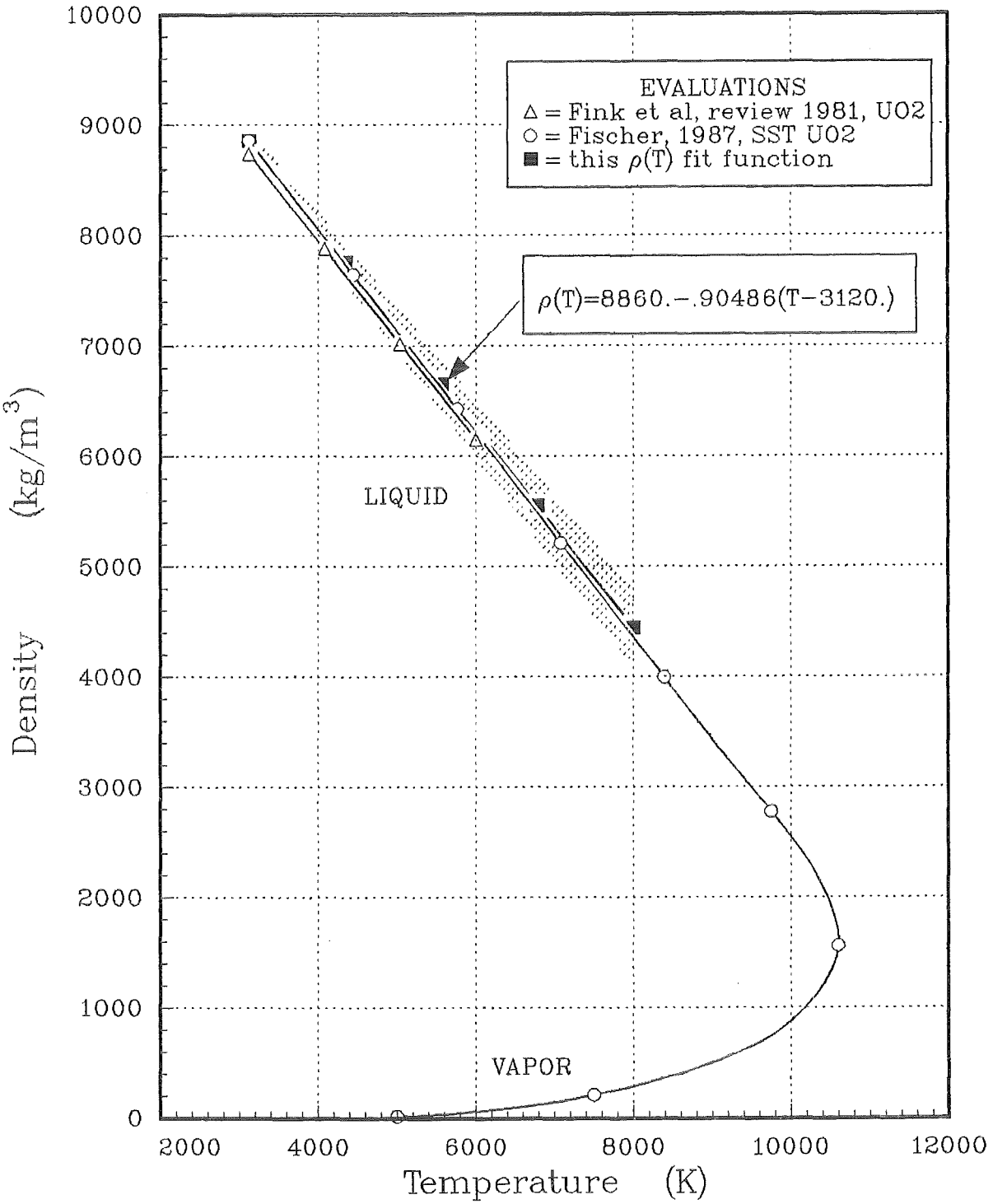

Figure 8: Comparison of the recommended ρ(T) fit function (Eq. 9) to earlier density evaluations for UO_2. Fischer's Significant Structures Theory (SST) model was anchored at Drotnings melt density (Ref. 8) and recent vapor pressure measurements (Ref. 1). The agreement between Eq. 9 and the SST results indicates good consistency between the measured data for the liquid and the vapor branch of the density curve.

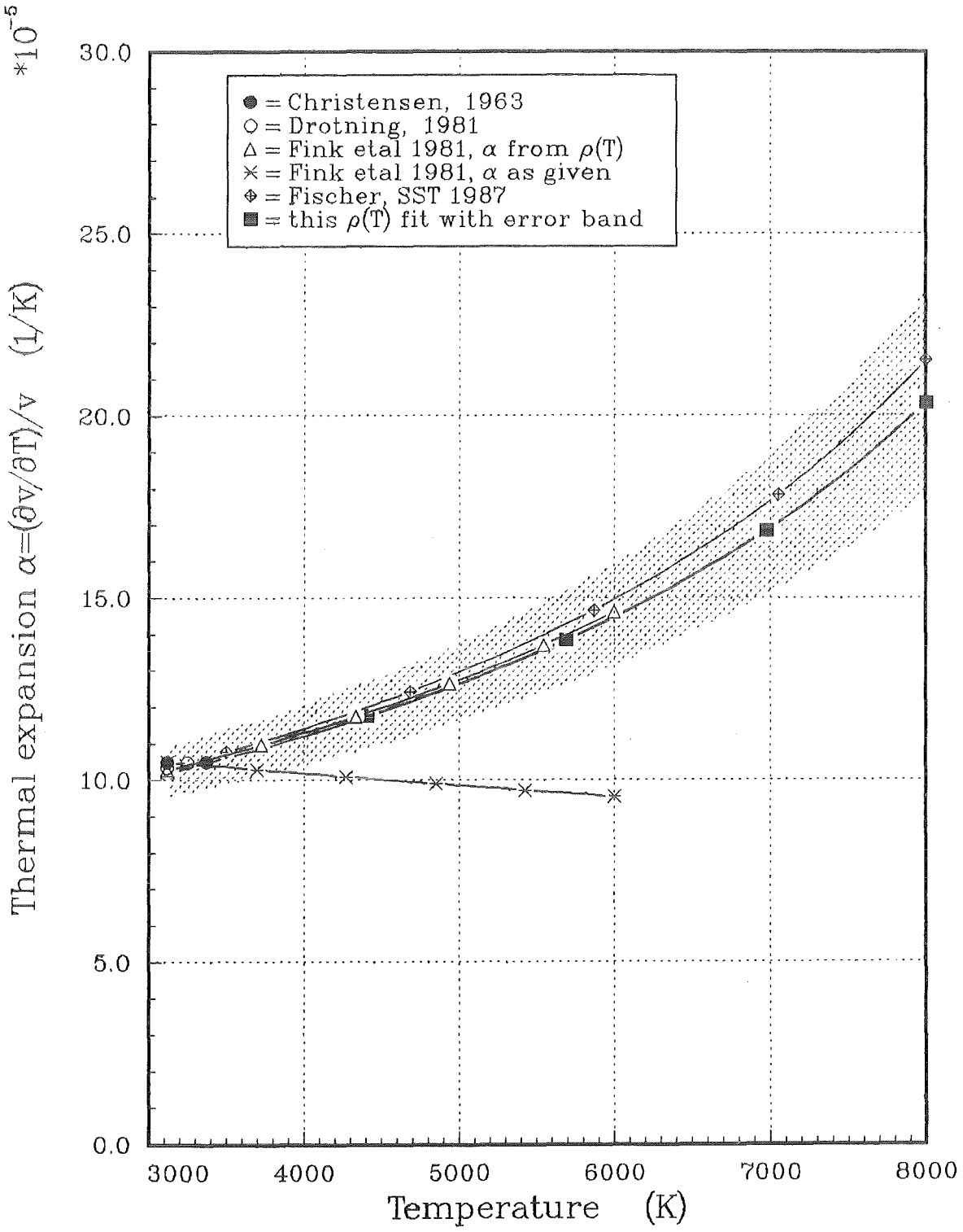

Figure 9: Summary of thermal expansion coefficients of UO_2 and $(U,Pu)O_2$. The recommended α(T) function and the shaded error band result from Eqs. (9) and (14). The shaded error band corresponds to the shaded area in Figure 8.

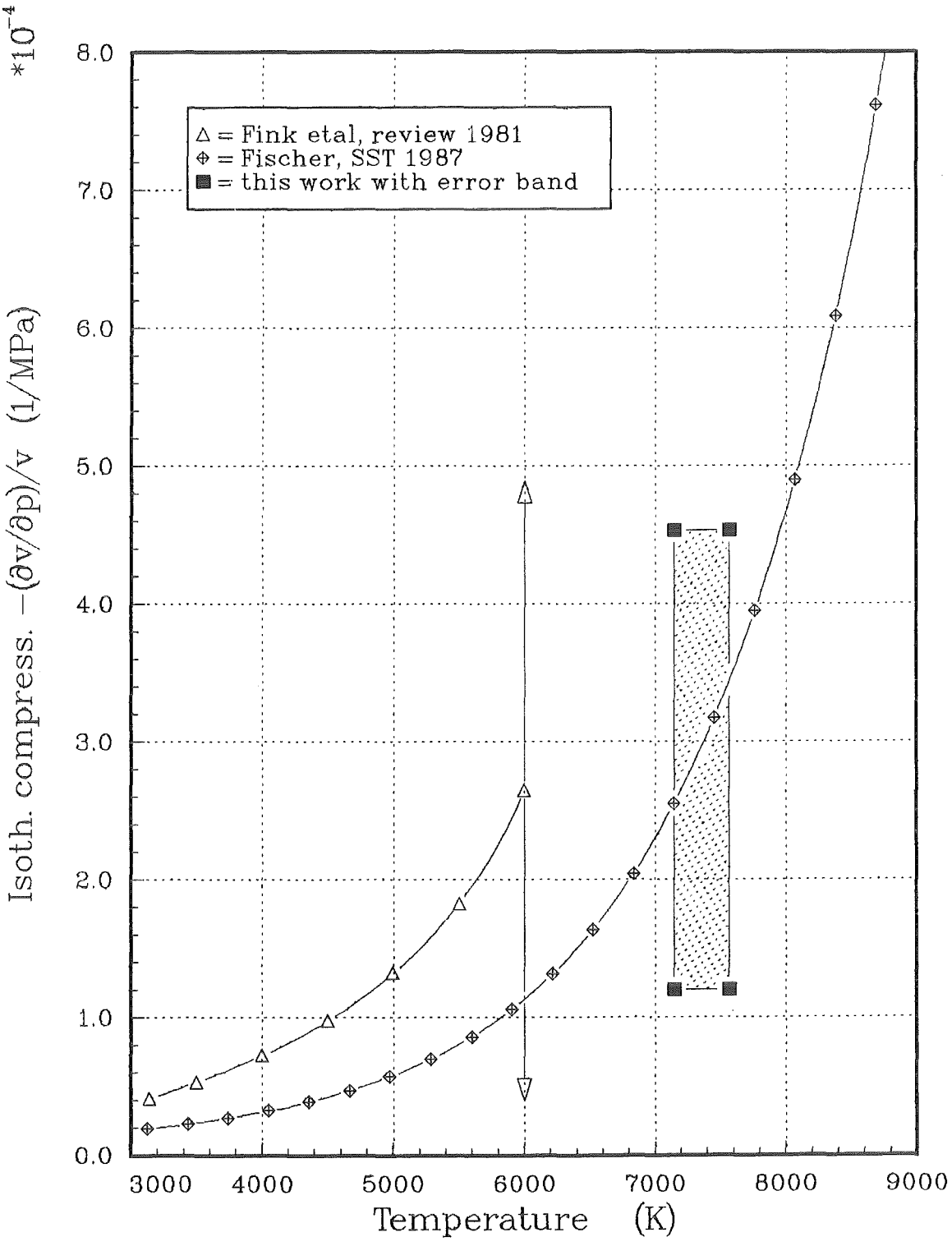

Figure 10: Comparison of measured isothermal compressibility data range to theoretical evaluations. All data are still subject to large uncertainties. The SST results appear to be the current best estimate for liquid oxide fuels because they are based on a detailed physical model and fall within the experimental data field.